Asian Journal of Chemistry; Vol. 35, No. 6 (2023), 1369-1378

ASIAN JOURNAL OF CHEMISTRY

https://doi.org/10.14233/ajchem.2023.27809

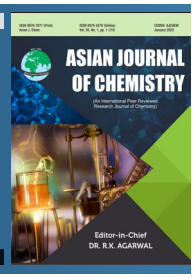


# Efficient Photodegradation of Methylene Blue using WLED with Nanosphere Graphitic Carbon Nitride Compared with its Bulk Counterpart

PINGAL SARMAH* and SONIT KUMAR GOGOI

Department of Chemistry, Gauhati University, Guwahati-781014, India

*Corresponding author: E-mail: pingal1988sarmah@gmail.com

*Received*: 1 April 2023; *Accepted*: 15 April 2023; *Published online*: 27 May 2023; AJC-21252

Herein, a simple solvothermal synthesis of graphitic carbon nitride nanosphere (*g*-CNN) at 180 ºC is reported. The photocatalytic activity of *g*-CNN was studied under an in-house developed white light emitting diode (WLED) reactor and characterized by FESEM, PXRD, FTIR, EDX, UV-visible spectroscopy and BET isotherm. The *g*-CNN has absorbance in visible light region and exhibits enhanced photocatalytic activity compared to bulk graphitic carbon nitride (BGCN) for photodegradation of methylene blue, which attributes to its lower surface area. The photocatalytic performance of *g*-CNN as function of pH of dye solution and catalyst amount were also studied. The *g*-CNN can be used for three repeated cycles with minimal change in photocatalytic efficiency. The solvothermal synthesis method at relative low temperature introduces terminal oxygen functionalities in *g*-CNN, which enhance light absorption and accelerate electron transfer results in improvement of photocatalytic efficiency of *g*-CNN. The results demonstrated the effectiveness of *g*-CNN as a photocatalyst for the treatment of water using visible light from WLED.

**Keywords: Graphitic carbon nitride, Nanosphere, Photocatalyst, Methylene blue, WLED.**

## INTRODUCTION

Industrial contaminants releasing continuously into the waterbodies degrade the quality of water day by day and rendering it toxic to human and environment. Textile industries are the biggest global water polluter followed by paint, leather and printing industries which discharge contaminated organic dyes such as methylene blue, crystal violet, methyl orange, *etc.* into the environment consistently [1]. This uncontrolled disposal of dye into water is dangerous to human health and aquatic life ecosystem as a whole. The consequences can be in the form of various carcinogenic, mutagenic and skin diseases in living beings [2-4].

Methylene blue is most commonly used in the industries for colouring silk, wool, paper, cotton, *etc*. It poses a number of dangers to human health, including those to the eyes, the lungs, the digestive system, and the brain [2]. Therefore, removal of methylene blue from industrial waste using different methods becomes an important and necessary topic of investigation. Methods that have been applied for this purpose includes membrane separation, ultrafiltration, photocatalytic degradation, electrocatalysis and adsorption process [5-9].

Photocatalytic degradation of dyes by developing different photoactive materials is one of the preferred technology among the researchers as it provides the scope of harnessing abundant solar energy which otherwise a solution to global energy crisis [11-12]. Though abundant, use of solar light in photocatalytic water treatment system has some limitations such as high installation cost, large surface area, requirement of skill for adjusting incidence direction and duration, *etc.* However, combination of artificial light sources with solar light may reduce the limitations of photocatalytic water treatment system. White light emitting diodes (WLEDs) can play a significant role in replacing mercury vapour or xenon lamps as the light source due to their lower cost and lower risk. Gogoi *et al*. [13] employed a 100 W light-emitting diode (LED) and found that gold nanoparticles supported on $TiO_2$ were an effective photocatalyst for ethanol oxidation. When it comes to photodegradation, employing visible light sources like WLEDs is more environmentally friendly than using ultraviolet light [14]. Therefore, WLEDs can be the future light source of photocatalytic water treatment.

Graphitic carbon nitride is the most stable allotrope of the carbon nitrides and, being a semiconducting material, belongs

to a broad category of photoactive substances. In literature, it is reported that the carbon nitrides are capable of reducing carbon dioxide [15-18], splitting water [15,19-23], degrading organic pollutants such as dyes [24-27] under illumination in the visible light range, as well as having a high sensitivity in sensing applications [26,28-31] and catalyzing organic reactions [32-35]. Graphitic carbon nitride is a metal free conjugated layered polymer material composed of carbon and nitrogen as primary elements. Various methods have been used for the synthesis of graphitic carbon nitride and the most common are condensation of appropriate nitrogen rich precursors such as urea, melamine, dicyanamide, cyanamide, thiocyanates, *etc*. at high calcination temperature of 400-600 ºC.

Paul *et al.* [36] studied the effect of calcination temperature on photodegradation of methylene blue dye for which graphitic carbon nitride was synthesized from urea at different temperatures. They found graphitic carbon nitride synthesized at higher temperature of 550 ºC shows better photocatalytic activity towards methylene blue degradation among the samples prepared in the range of temperature from 350 to 750 ºC. Actually condensation synthesis of graphitic carbon nitride is only possible in a small temperature range of 500 to 600 ºC. Montigaud *et al.* [37] also tried to synthesize graphitic carbon nitride at comparatively low temperature using solvothermal condensation of melamine with cyanuric chloride. Xie *et al.* [38] also synthesized graphitic carbon nitride solvothermally from cyanuric chloride and sodium amide in benzene by heating at 200 ºC for 8-12 h. Bai *et al.* [39] also synthesized crystallized graphitic carbon nitride by the reaction of carbon tetrachloride and ammonium chloride at 400 ºC. Graphitic carbon nitride has interesting properties, but researchers are continously taking efforts to synthesize it at low temperature.

In this work, we have successfully synthesized *g*-CNN by a simple one step solvothermal method at 180 ºC. The morphology, crystallinity, surface area, chemical and elemental composition of *g*-CNN were also investigated. The photodegradtion ability of synthesized *g*-CNN was studied using methylene blue dye in aqueous medium under WLEDs and compared with bulk graphitic carbon nitride (BGCN), which was synthesized at high calcination temperature and characterized well to carry out the comparative studies.

## EXPERIMENTAL

Cyanuric chloride, cyanamide, melamine, acetonitrile and methylene blue were bought from Merck Specialities Pvt. Ltd., India and used as received. Distilled water and Whatman-40 filter paper was used for all the experiments. Photocatalytic experimental setup was built in the laboratory for which five 20 W WLEDs and a 12 V adaptor were bought from the local electrical market.

**Synthesis of graphitic carbon nitride nanosphere (*g*-CNN) and bulk graphitic carbon nitride (BGCN):** In a typical synthetic procedure, 7.5 mmol (1.383 g) cyanuric chloride and 7.5 mmol (0.347 g) cyanamide were dispersed in 30 mL acetonitrile and stirred for 15 min. The mixture was then transferred to a Teflon lined autoclave and heated to 180 ºC for 14 h. After the autoclave cooled to room temperature, yellow precipitate was obtained which is filtered, washed many times with distilled water and dried overnight for further use. For comparison bulk graphitic carbon nitride was synthesized by following the reported method [40]. Melamine (5 g) was placed in a muffle furnace at 550 ºC for 4 h. After cooling to room temperature naturally, yellow coloured BGCN was obtained, ground into powder using agate mortar. The as-prepared BGCN was characterized and used further.

**Photocatalysis experiments:** The photocatalytic degradation of aqueous methylene blue solution by *g*-CNN and BGCN were carried out under a simple, low cost experimental set up developed in our laboratory [41]. In brief, 30 mg of catalyst was dispersed in 30 mL of $10^{-5}$ M aqueous solution of methylene blue dye and stirred in dark for 60 min to allow methylene blue adsorption-desorption equilibrium on the *g*-CNN surface after which the suspension was irradiated with WLEDs under continuous magnetic stirring. The UV-visible spectroscopy was used to track the progress of the photocatalytic degradation of methylene blue in 2 mL aliquots of the samples at regular intervals. To maintain a constant volume in the reaction, the solution was added after the measurement was taken The photocatalysis experiment was carried out at three different pHs *viz*. 4.2, 6.7 and 11.3 of methylene blue solution. The effect on degradation efficiency by varying catalyst amount and kinetics were studied. A control experiment was also conducted to observe the effect of light without the addition of a catalyst.

**Recyclability studies:** Two different procedures were used to test the recyclability of catalyst. First, a photocatalytic degradation for the first recycle was initiated by using the same experimental conditions as the initial photocatalytic experiment between methylene blue and fresh catalyst, which involved the addition of a calculated amount of methylene blue dye from stock to achieve the same absorbance as in the initial experiment. This method was repeated for three recycles since, it reduces the chance of catalyst lost during recovery. The second method involved the collection of catalyst once each photodegradation cycle was complete. The catalyst was left in the reaction beaker overnight after each cycle to settle, then the supernatant solution was decanted next day. Recovered catalyst was subsequently rinsed in water, dried and recycled. To monitor the loss over time, the dried catalyst was weighed after each cycle.

**Characterization:** The morphology and size of the samples were analyzed by field emission scanning microscope (FESEM, ZEISS Sigma-300). The elemental composition of the samples were recorded by energy dispersive X-ray (EDX) attached to FESEM. The powder X-ray diffraction pattern (PXRD) of the samples are recorded from 5º to 80º (2θ) on a Rigaku Ultima IV X-ray diffractometer with Cu*K*α radiation (λ = 1.54 Å). Fourier transformed infrared spectroscopy (FT-IR) spectra were recorded on Shimadzu IR Affinity-1 in the range from 500 to 4000 $cm^{-1}$ with KBr pellets. The diffuse-reflectance UV-Vis-NIR spectra were recorded using a Shimadzu UV-2600 spectrophotometer in the range 200-1500 nm. UV 1800 spectrophotometer (Shimadzu, Japan) was used for recording UV-visible absorption of methylene blue solution from 200 to 800 nm. The surface area of the sample was recorded in Quantachrome Instruments, Model- NOVA 1000E.

## RESULTS AND DISCUSSION

**FTIR studies:** The FT-IR spectra of *g*-CNN and BGCN shows similar adsorption bands are presented in Fig. 1. The BGCN show peaks at 1558 and 1408 $cm^{-1}$ are attributed to stretching vibrations of C=N. The peaks at 1319 and 1230 $cm^{-1}$ of BGCN and 1454 and 1357 $cm^{-1}$ of *g*-CNN are assigned for aromatic C-N stretching vibrations [42]. The peaks at 1730 and 1634 $cm^{-1}$ of *g*-CNN are due to stretching vibrations of C=O. The characteristic peak at 804 $cm^{-1}$ of BGCN corresponds to the breathing mode of triazine ring, whereas in *g*-CNN this peak slightly shifted to 796 $cm^{-1}$ due to the incorporation of oxygen moieties [43].

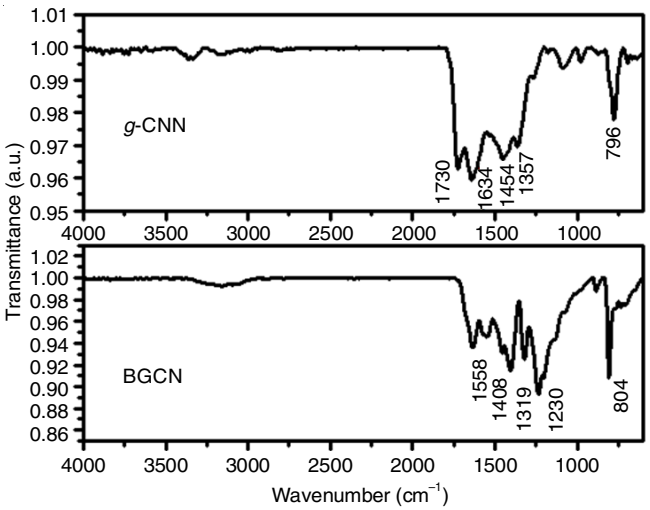


Fig. 1. FT-IR spectra of *g*-CNN and BGCN

**Morphological studies:** The morphology of *g*-CNN and BGCN were analyzed by FESEM. As evident from the FESEM images, the *g*-CNNs are spherical in shape, Fig. 2a and BGCN shows stacking of multiple layers, resulting a thick structure (Fig. 2b). The PXRD patterns of *g*-CNN and BGCN are shown in Fig. 3. Both BGCN and *g*-CNN show strong peaks at 27.4º and 27.7º, respectively. These are the characteristic peak of inter planar stacking of conjugated triazine layers and indexed for graphitic material as (002) peak [44]. The slight shifting

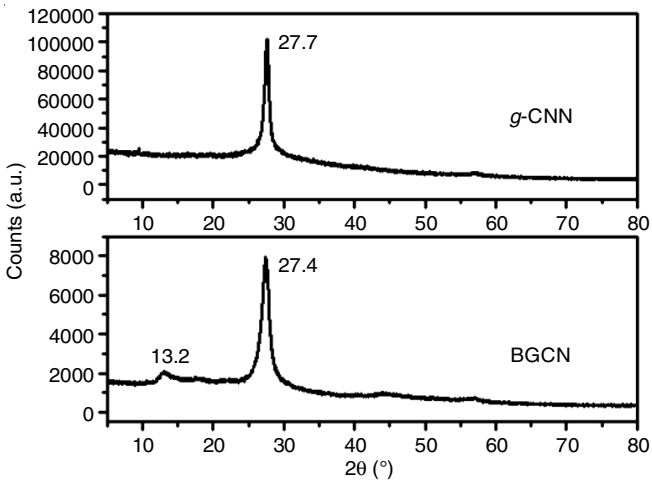


Fig. 3. PXRD patterns of *g*-CNN and BGCN

of (002) peak in *g*-CNN depicts denser packing and improved order of stacking between the layers *via* π-π interactions [36]. BGCN shows a low angle peak at 13.2º originated from in planar repeated triazine units indexed for (100) plane. This peak is absent in the PXRD pattern of *g*-CNN suggests relative lower polymerization degree of carbon nitrde than from calcination synthesis at high temperature [45].

The EDX spectrum, Fig. 4a,b (inset: corresponding elemental composition table), gives the elemental composition of BGCN as C = 60.84 %, N = 38.37 %, O = 0.79 % and *g*-CNN as C = 25.89 %, N = 38.33 %, O = 35.78 %. The increase % of O in *g*-CNN is also reflected in its FTIR spectrum, higher oxygen functionalities could be observed like 1730 & 1634 $cm^{-1}$, which correspond to different carbonyl groups. This is due to the fact that at lower temperature (180 ºC), the carbon nitride polymerization is not complete and the structures formed have terminal functional groups. As the synthesis is carried out under arieal conditions oxygenated functional groups are inevitable. While BGCN was prepared at higher temperature of 550 ºC, at this temperature the polymerization of the precursors/intermediates (such as melamine, urea, thiourea, guanidine hydrochloride, *etc.*) to form carbon nitride was completed to a greater degree, leaving less percentage of terminal functional groups compared to the *g*-CNN [46].

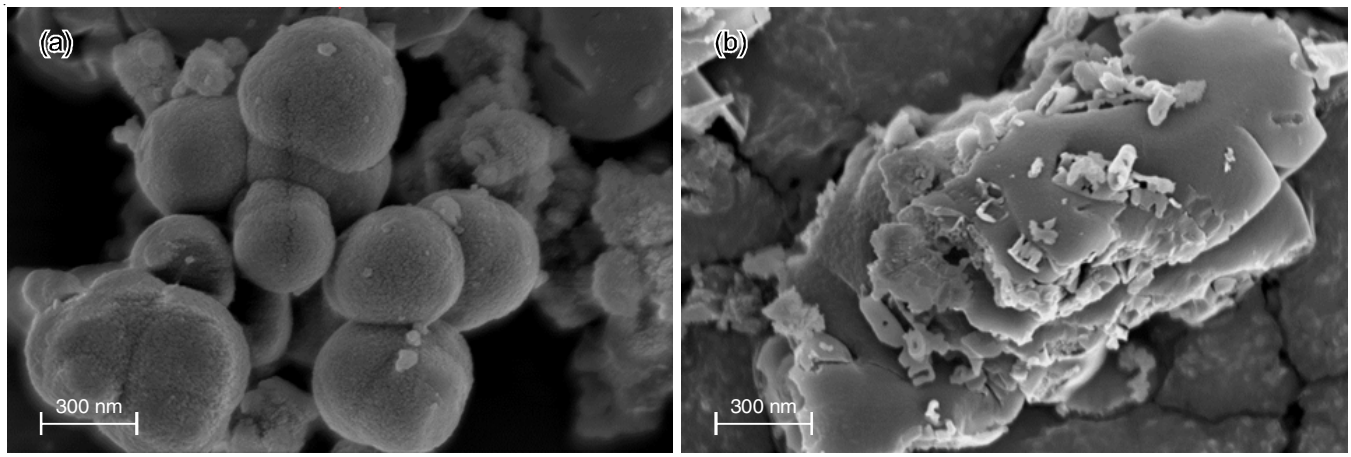


Fig. 2. FESEM images of (a) *g*-CNN and (b) BGCN

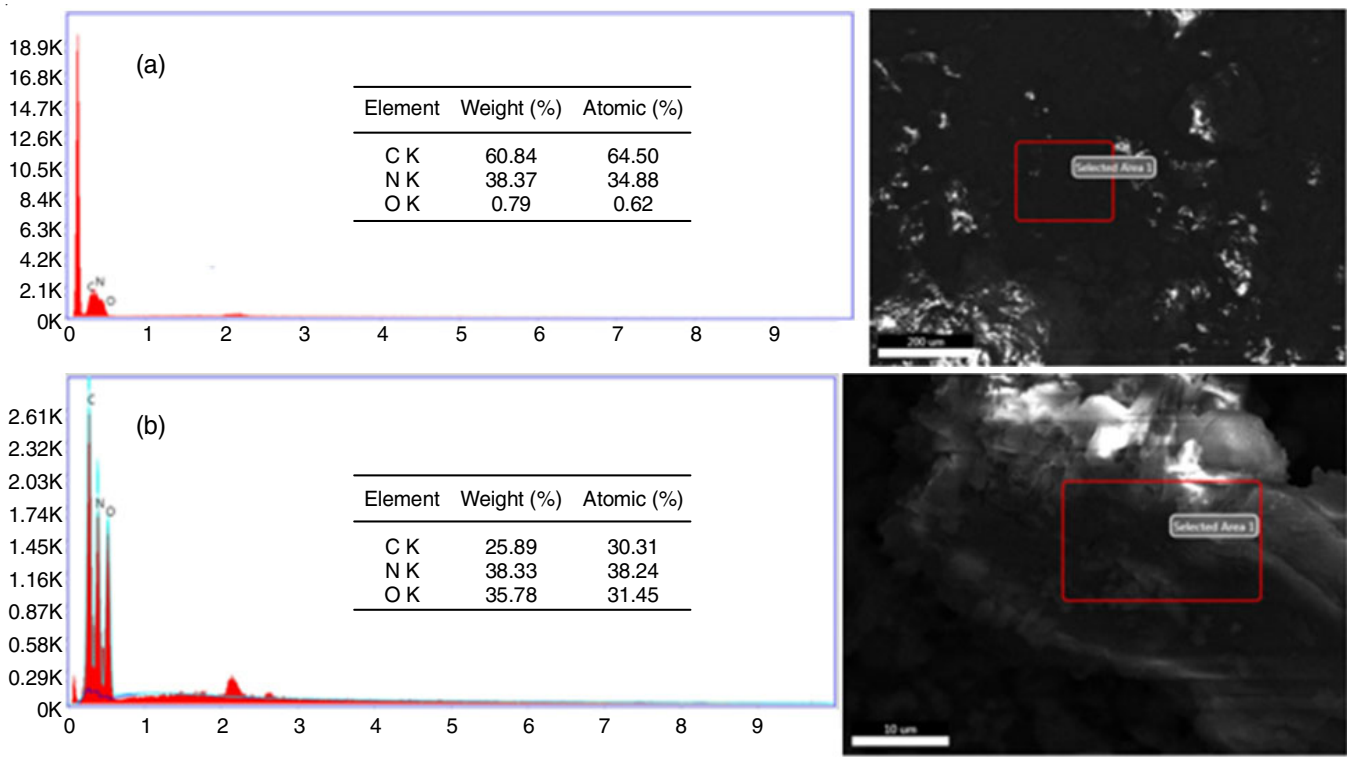


Fig. 4. EDX spectrum of (a) BGCN and (b) *g*-CNN

**UV-visible-DRS studies:** The DRS spectra of *g*-CNN and BGCN are shown in Fig. 5a and the corresponding energy gap in the inset. Broader absorbance of *g*-CNN compared to BGCN may also be related to the higher percentage of terminal functional groups in *g*-CNN giving greater potential of *g*-CNN as visible light driven photocatalyst [46]. The energy band gap of *g*-CNN is smaller than BGCN, 2.43 and 2.72 eV respectively, which is estimated from Tauc plot.

**BET surface studies:** The specific surface area of *g*-CNN was determined by $N_2$ adsorption-desorption isotherm (Fig. 5b). The BET surface area of the *g*-CNN is found to be 23.31 ($m^2$/g) which is 1.7 times higher than the bulk graphitic carbon nitride synthesized by Praus *et al.* [40]. In their study, the photocatalytic activity of bulk graphitic carbon nitride synthesized by heating melamine at 550 ºC for 4 h in the air and nitrogen atmosphere was checked for which the specific surface area of bulk graphitic carbon nitride was found to be 14 $m^2$/g.

**Photocatalytic studies:** The photocatalytic activity of *g*-CNN and BGCN towards photodegradation of methylene blue dye was studied under the visible light irradiation of WLEDs (100 W). As observed from Fig. 6a-b, *g*-CNN shows better photocatalytic activity than BGCN. The *g*-CNN degrades

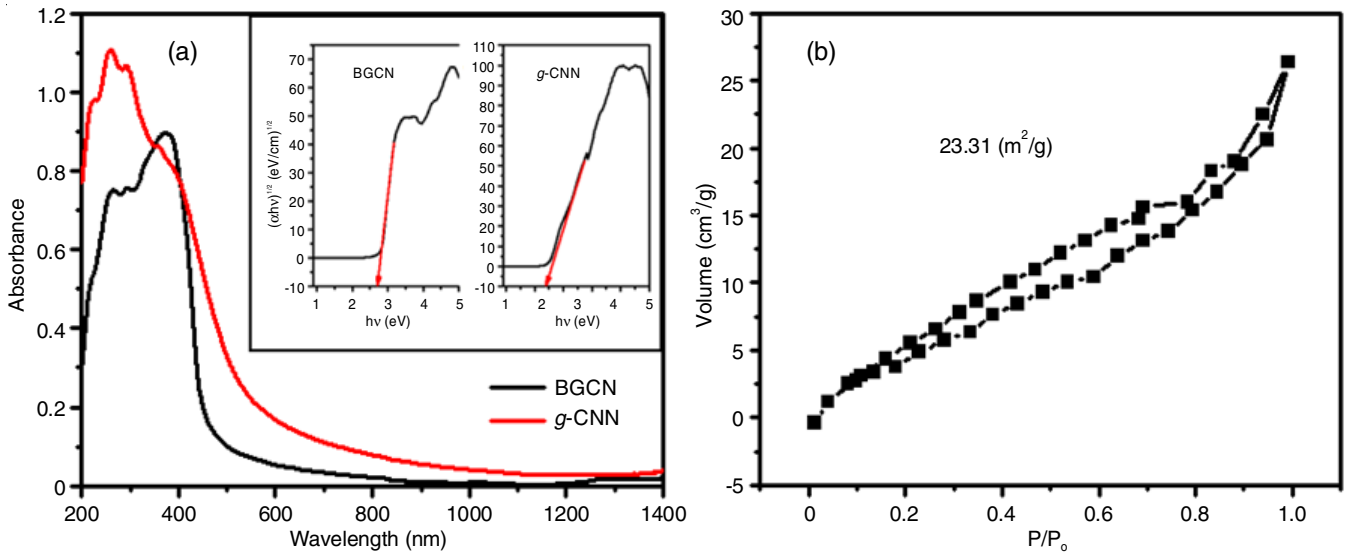


Fig. 5. (a) UV-visible DRS spectra of *g*-CNN and BGCN, inset energy band gap of BGCN and *g*-CNN using Tauc's plot, (b) $N_2$ adsorption-desorption isotherm of *g*-CNN (inset: BET surface area)

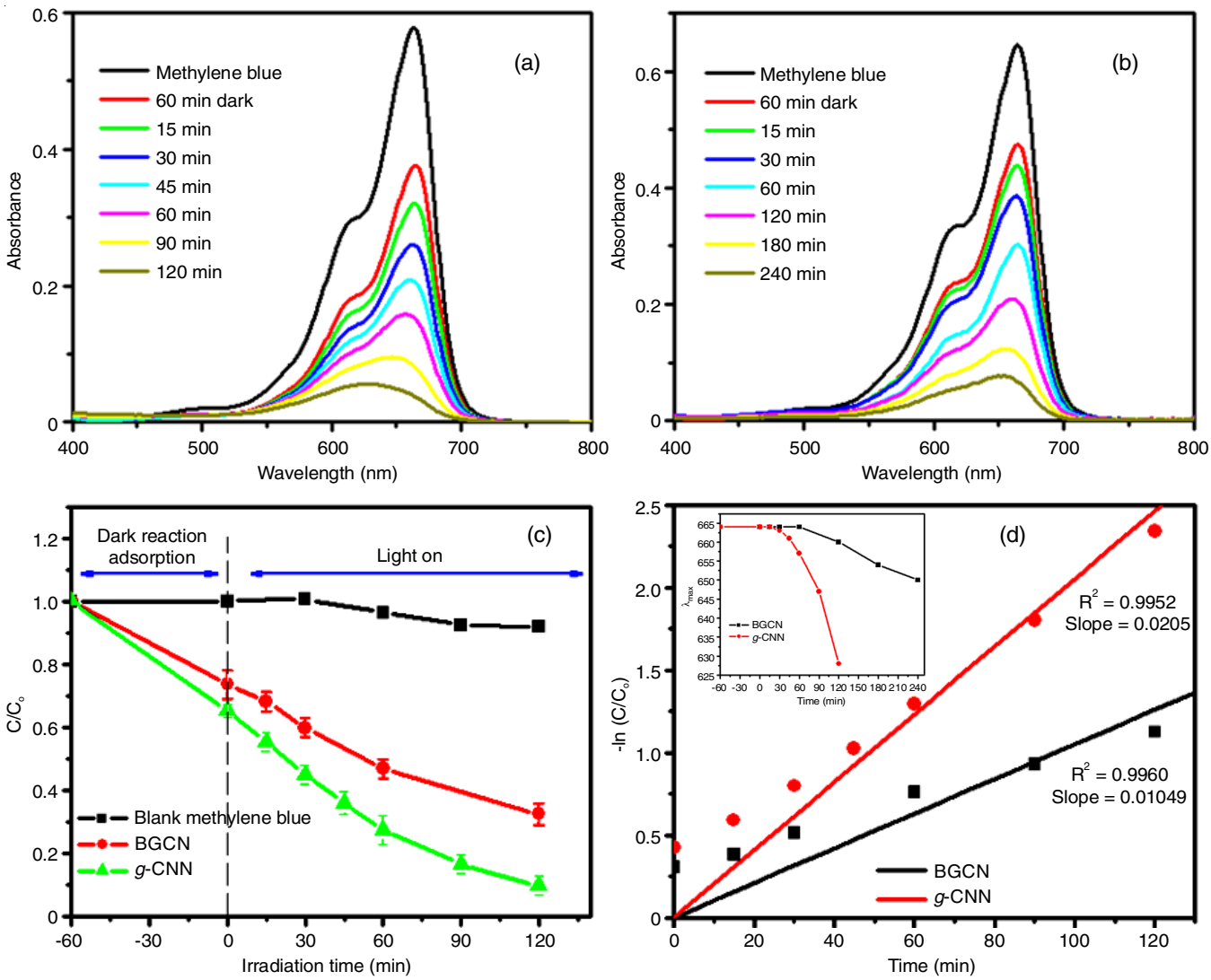


Fig. 6. UV-visible spectra of aqueous solution of methylene blue ($10^{-5}$ M) at different time interval in presence of (a) *g*-CNN and (b) BGCN, (c) Photocatalytic activity of degradation of methylene blue, C/C$_o$ *vs.* irradiation time plots, (d) The corresponding reaction kinetics fitted –ln (C/C$_o$) *vs.* time plots, inset shift in $\lambda_{max}$ of methylene blue during photodegradation

90.36% of methylene blue in 120 min while BGCN degrades 88.06% of methylene blue in 240 min under similar experimental conditions. The photocatalytic degradation efficiency was calculated using the following equation:

$$E = 1 - \frac{C}{C_o} \times 100\%$$

where C is the concentration of the solution at time t, $C_o$ is the initial concentration of solution at zero time. The exponential decay observed in the C/C$_0$ *vs.* time plot (Fig. 6c), which indicates that the photodegradtion of methylene blue by the catalysts follow pseudo-first order reaction kinetics. The pseudo-first order rate constant can be determined following the equation:

$$-\ln\frac{C}{C_o} = k_s \times t$$

where $k_s$ is the pseudo-first order rate constant and t is the reaction time [36]. The rate constants for photocatalysis of methylene blue by BGCN and *g*-CNN were $1.1 \times 10^{-2}$ min$^{-1}$ and $2.1 \times 10^{-2}$ min$^{-1}$, respectively, a 2.3 fold increase in photcatalytic activity is observed, Fig. 6d (inset shift in $\lambda_{max}$ of methylene blue during photodegradation).

**Mechanism:** As shown in **Scheme-I**, during the photocatalysis of methylene blue dye, light of suitable photon energy *i.e.* higher than energy band gap of *g*-CNN falls over its surface, electrons in the valence band get excited to conduction band by absorbing light, generating holes in valence band and free electrons in conduction band. These hole-electron generation and associated charge separation plays the key role in the photocatalysis reaction. The holes with high oxidative potential either direct oxidize the dye or react with $OH^-$ to form hydroxyl radical ($^\bullet OH$) that degrades dye molecules. The free electrons produced are picked up by oxygen to generate super oxide radical anion ($^\bullet O_2^-$) which can also lead to photodegradation of methylene blue molecules.

$$g\text{-CNN} + h\nu \longrightarrow g\text{-CNN} + (h^+ + e^-)$$

$$O_2 + e^- \longrightarrow {}^\bullet O_2^-$$

$$h^+ + \text{dye} \longrightarrow {}^\bullet \text{Dye}^+ \text{ (oxidation of dye)}$$

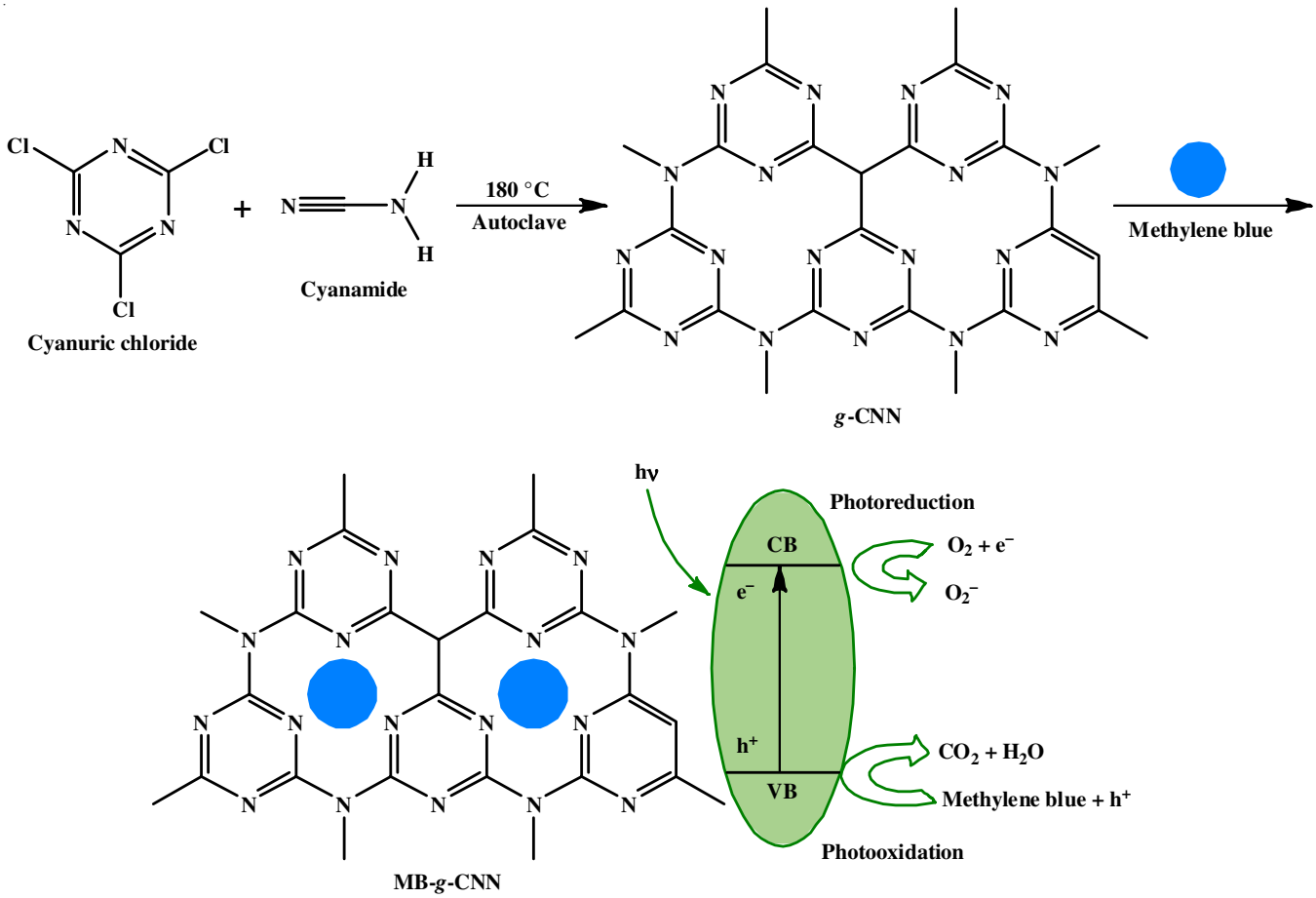


**Scheme-I:** Synthetic scheme of graphitic carbon nitride and its application for photocatalytic degradation of methylene blue from aqueous medium

or $h^+ + OH^- \longrightarrow {}^\bullet OH$

${}^\bullet OH + \text{dye} \longrightarrow \text{Degradation of dye}$

The nanosphere of *g*-CNN provides more surface area, resulting in increased density of active sites to adsorb more numbers methylene blue molecules for the photodegradation, confirmed by FESEM images and BET surface area measurement of *g*-CNN. Smaller energy band gap of *g*-CNN (2.43 eV) compared to BGCN (2.73 eV), calculated using Tauc's plot confirms the smooth transfer of electrons-holes between valence and conduction band of *g*-CNN when exposed to visible light. This electon-hole generation initiate the photoredox reaction and methylene blue molecules that are adsorbed on the surface of *g*-CNN undergo photodegradation. The XRD analysis revealed that synthesis of the *g*-CNN at lower temperature reduces the chance of high polymerization. On the other hand, BGCN which was synthesized at high calcination temperature undergo high polymerization degree of carbon nitride making the structure excessively condensed into deformed multilayered, which reduces the exposure of active sites in the material. This affect the photocatalytic ability of BGCN adversely. High calcination temperature in the synthesis also induce bulking and thermal decomposition of polymeric material as well. The FTIR and EDX analysis confirms the incorporation of oxygen functionalities in *g*-CNN can enhance the light absorption, which is reflected in DRS spectrum of the sample also, accelerate the electron transfer so as to improve the photocatalytic efficiency. Hence, the *g*-CNN synthesized at lower temperature shows the superior photocatlytic activity as compared to BGCN that synthesized at high calcination temperature.

It is observed that the photocatalytic degradation process of pollutants got pronouncedly affected by pH of the solution. Therefore, the photocatalytic activity of synthesized *g*-CNN was further analyzed at three different pHs, acidic (pH = 4.2), near neutral (pH = 6.7) and basic (pH = 11.3) by adjusting the dye solution with dil. solution of HCl and NaOH. Corresponding UV-Vis spectra are shown in Fig. 7a-c.

It is observed that when the pH value of methylene blue solution is set at 4.2 lesser than the neutral pH, the photoactivity of *g*-CNN decreases whereas on increasing pH value from the neutral in the basic range (pH = 11.3), a rise in the photoactivity of *g*-CNN is observed (Fig. 8a-b). The synthesized *g*-CNN shows the highest degradation efficiency of 97.33% for the methylene blue dye solution at pH 11.3, which is 1.4 times higher than the degradation efficiency at the neutral pH condition. This observation might be related to the adsorption behaviour of methylene blue on the surface of *g*-CNN. At high pH value the surface of *g*-CNN carries more negative charges and attracts more methylene blue molecules which bears positive ion. More the methylene blue molecules on *g*-CNN surface, more photodegradtion will occur. Another reason may be that at basic pH condition $OH^-$ can act as a capture agent for $h^+$, which generates

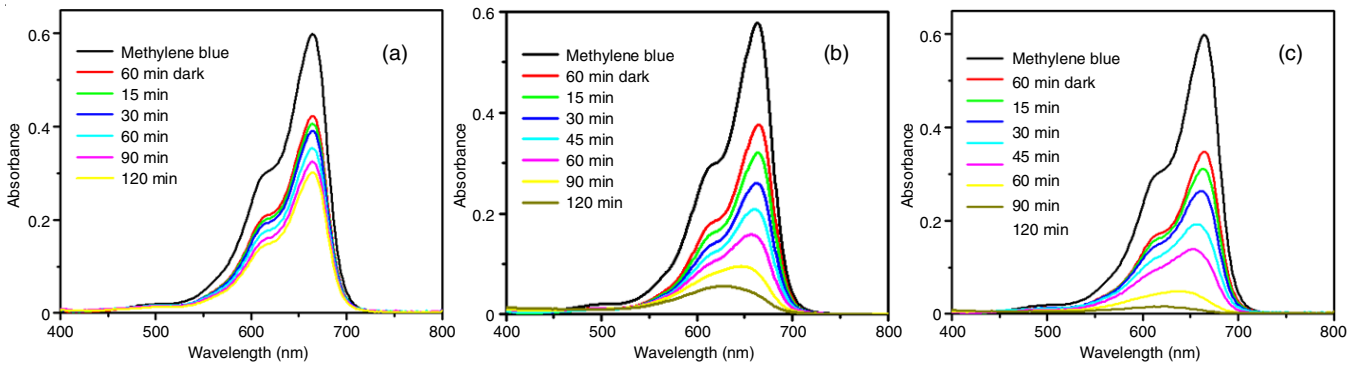


Fig. 7. UV-visible spectra of aqueous solution of methylene blue ($10^{-5}$ M) with *g*-CNN concentration of 30 mg/30 mL at different pH (a) pH = 4.2, (b) pH = 6.7 and (c) pH = 11.3

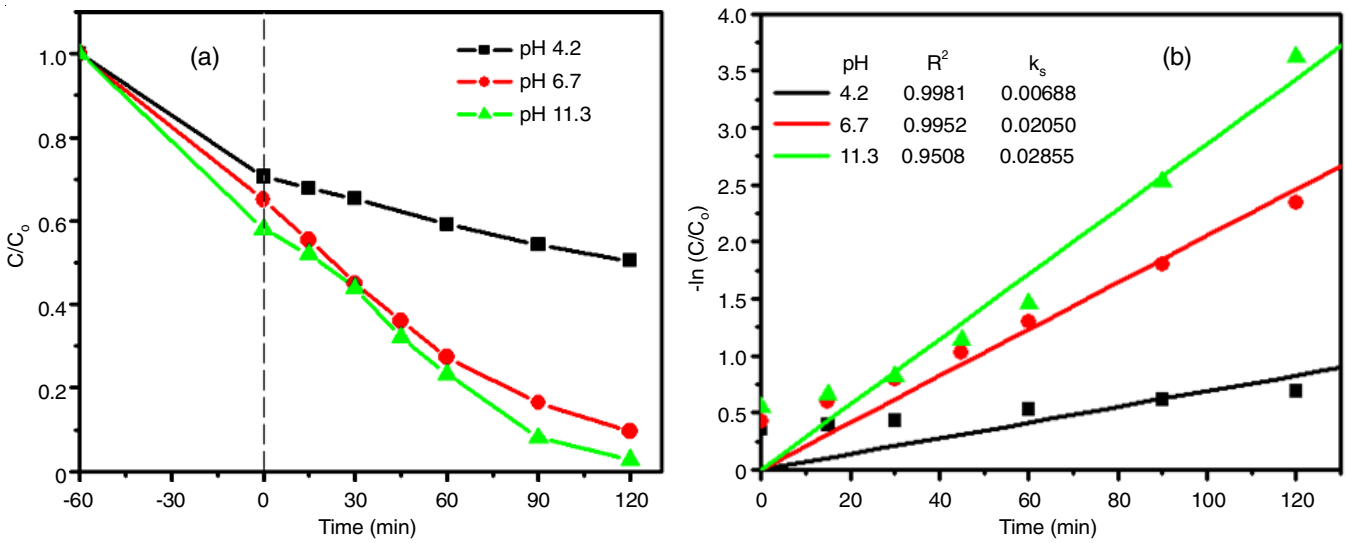


Fig. 8. (a) Comparison of photocatalytic activity of *g*-CNN with concentration 30 mg/30 mL at different pH condition (b) –ln ($C/C_o$) *vs.* time plot for methylene blue degradation with *g*-CNN at different pH conditions

$OH^{\bullet}$. So an increase in pH reduces the recombination probability for photogenerated electrons and holes, which enhances the photocatalytic activity [47]. The degradation efficiency and apparent rate constant measured for the photocatalytic reactions at three different pH conditions are presented in Table-1.

TABLE-1
DEGRADATION EFFICIENCY AND THE APPARENT RATE CONSTANT (k) VALUES MEASURED FOR THE PHOTOCATALYTIC REACTIONS AT DIFFERENT pH CONDITIONS

| pH value | Degradation efficiency (%) | Apparent rate constant (k) ($min^{-1}$) |
|---|---|---|
| 4.2 | 49.52 | 0.00688 |
| 6.7 | 90.36 | 0.02050 |
| 11.3 | 97.33 | 0.02855 |

Furthermore to investigate the effect of catalyst concentration on the photocatalytic activity of *g*-CNN towards methylene blue dye, the concentration of *g*-CNN was varied from 10 to 70 mg per 30 mL of $10^{-5}$ M methylene blue solution and related UV-Vis spectra are shown in Fig. 9a-d.

The photocatalytic activity was shown to increase from 10 mg to 50 mg of *g*-CNN, likely as a result of the higher concentration of active sites on the catalyst surface. The phenomena of light scattering may predominate at greater catalyst amounts, such that increasing the amount of catalyst beyond 50 mg may reduce activity by blocking the light path to reach the methylene blue molecules. As shown in Fig. 10a-b, 50 mg/30 mL concentration *g*-CNN showed highest degradation efficiency of 92.4% with rate constant 0.02405 $min^{-1}$ in 120 min for methylene blue dye solution. The percent degradation efficiency and the apparent rate constant measured for the photocatalytic reactions at different photocatalyst concentration are presented in Table-2.

TABLE-2
DEGRADATION EFFICIENCY AND THE APPARENT RATE CONSTANT (k) VALUES MEASURED FOR THE PHOTOCATALYTIC REACTIONS AT DIFFERENT PHOTOCATALYST CONCENTRATION

| Catalyst conc. (mg/30 mL of $10^{-5}$ M MB solution) | Degradation efficiency (%) | Apparent rate constant (k) ($min^{-1}$) |
|---|---|---|
| 10 | 42.82 | 0.00535 |
| 30 | 90.36 | 0.02050 |
| 50 | 92.40 | 0.02405 |
| 70 | 76.79 | 0.14540 |

MB = Methylene blue

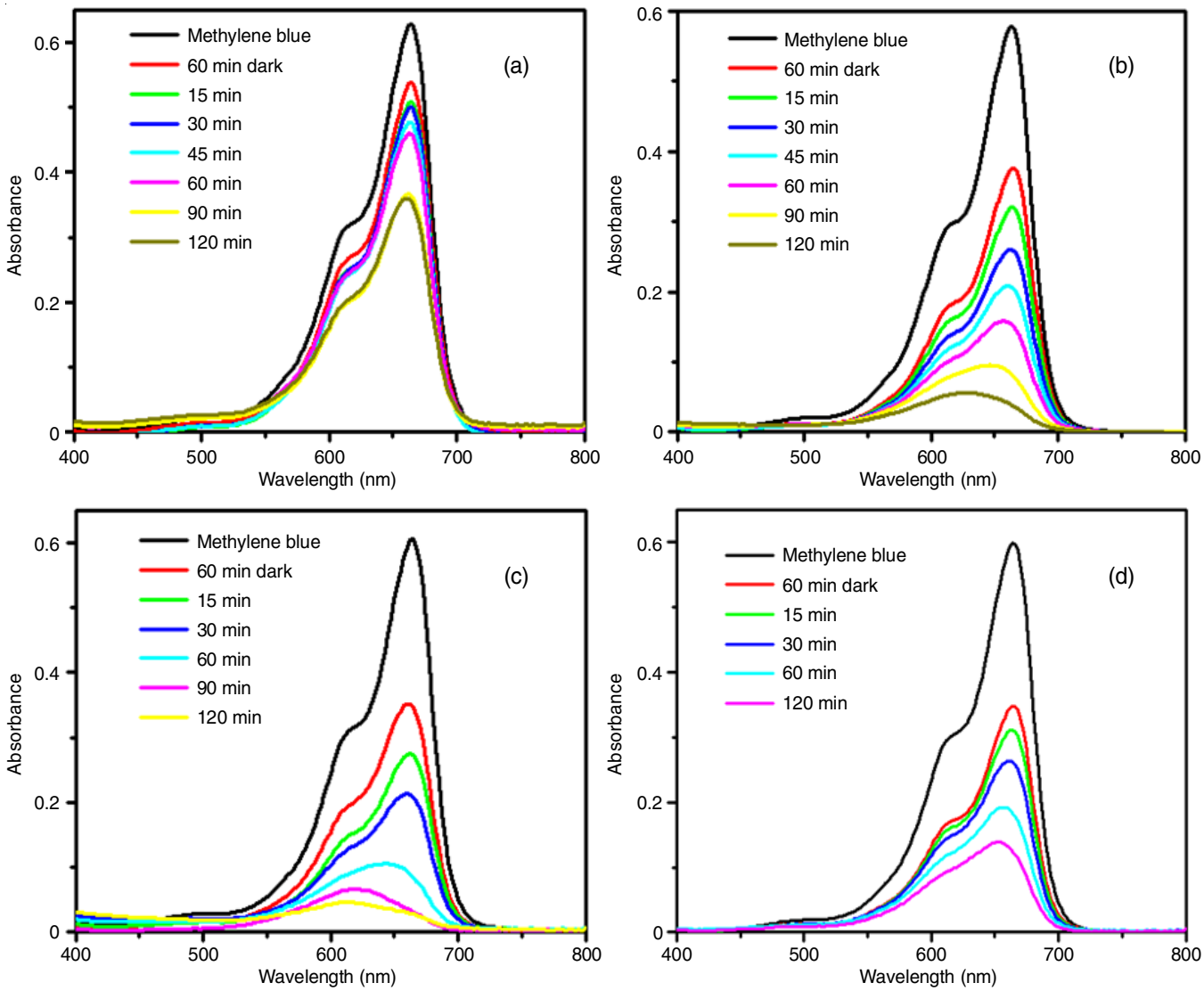


Fig. 9. UV-visible spectra of aqueous solution of methylene blue ($10^{-5}$ M) at different *g*-CNN concentration (a) 10 mg/30 mL, (b) 30 mg/30 mL, (c) 50 mg/30 mL and (d) 70 mg/30 mL

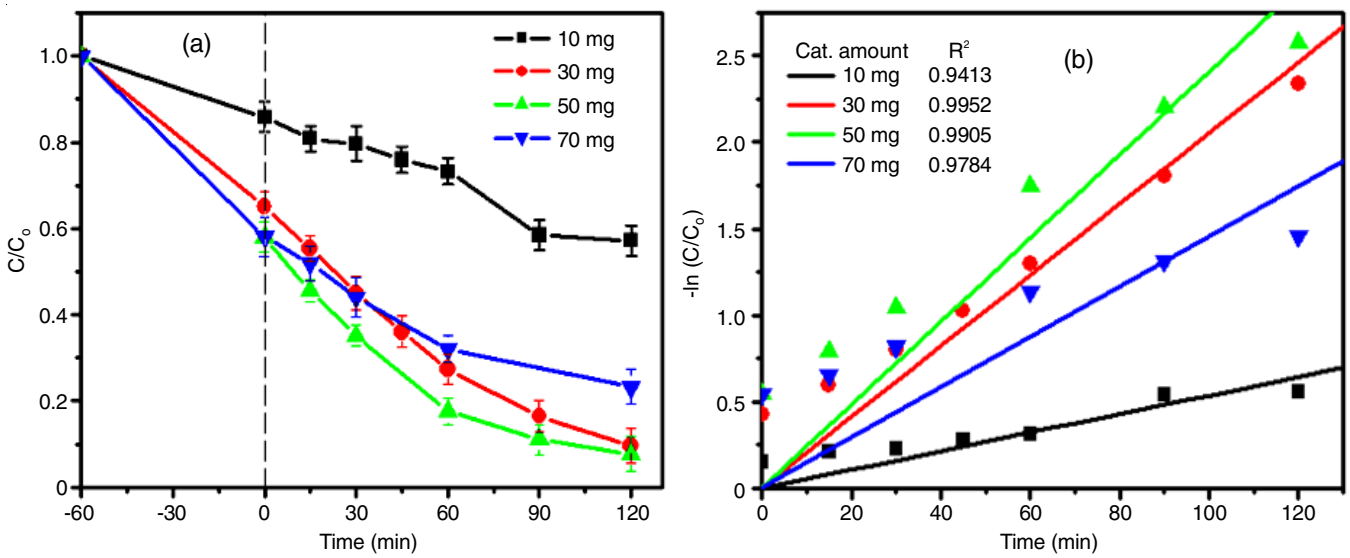


Fig. 10. (a) Comparison of photocatalytic activity of *g*-CNN at different catalyst concentration, (b) –ln ($C/C_0$) *vs.* time plot for methylene blue degradation with *g*-CNN at different catalyst concentration

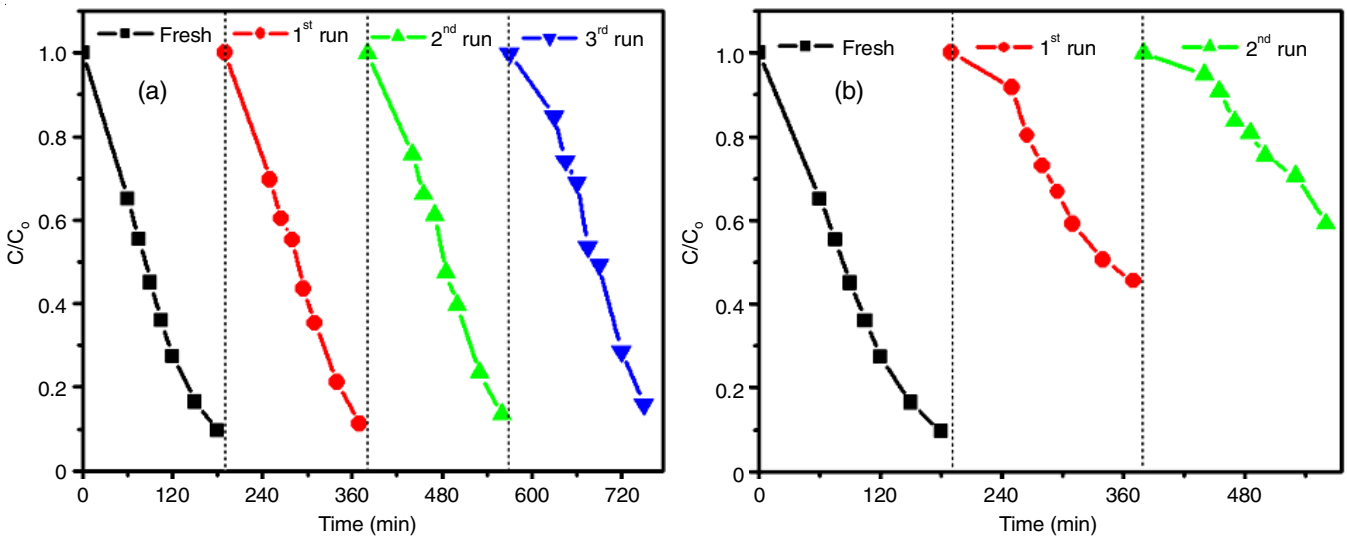


Fig. 11. Recyclability experiment of the photocatalytic degradation of methylene blue using *g*-CNN (a) 1st method (b) 2nd method

**Recyclability studies:** Two methods were used to evaluate the recyclable efficiency of *g*-CNN photocatalyst. The results from the first method are represented in Fig. 11a. The photocatalytic activity of *g*-CNN showed just a minor reduction in this case, from 90.36% with the catalyst to 84.58% methylene blue photodegradation in the third recycling. This demonstrates that after several cycles, *g*-CNN still maintains its high photocatalytic activity. The proportion of methylene blue degraded was found to decrease with each cycle of the second approach (Table-3), likely as a result of photocatalyst being lost during the recovery process. While the initial cycle of catalyst was able to degrade 90.36% of methylene blue in 120 min, the final cycle only managed to degrade 40.86%. Nonetheless, further cycles show essentially no change in the degradation rate per milligramm of the catalyst as seen in the final column of Table-3. Thus, in both techniques, the catalyst activity was stable throughout the multiple cycles.

TABLE-3
COMPARISON OF DEGRADATION OF METHYLENE BLUE AT DIFFERENT CYCLES (SECOND METHOD)

| Cycles of experiment | Recovered amount of catalyst (mg) | Degradation efficiency (%) | % Degradation per mg of *g*-CNN |
|---|---|---|---|
| Fresh | 30 | 90.36 | 3.012 |
| Cycle 1 | 22 | 63.23 | 2.874 |
| Cycle 2 | 14 | 40.86 | 2.724 |

## Conclusion

In summary, graphitic carbon nitride nanosphere (*g*-CNN) was synthesized by following a simple solvothermal method at low temperature (180 ºC) using cyanuric chloride and cyanamide as precursors. The photocatalytic performance of as synthesized *g*-CNN towards methylene blue degradation has compared with BGCN synthesized at high calcination temperature (550 ºC) from melamine. An increase in the photocatalytic activity by 2.3 fold was observed in case of *g*-CNN synthesized at lower temperature. This was due to the more surface area and smaller band gap of *g*-CNN where presence of oxygen bearing groups can increase absorption of light compared to BGCN. The photocatalytic activity of *g*-CNN was highest at the basic pH condition of dye solution. This was attributed to the high adsorption of positive charge bearing methylene blue on more negative *g*-CNN surface. The percentage of methylene blue degradation increases with the increase of *g*-CNN amount from 10 mg to 50 mg but thereafter it decreases, which is due to the hindrance in entering light in the reaction system. The *g*-CNN photocatalytically degraded methylene blue upto 90.36 % within 120 min and can be repeated for atleast three cycles. This study inferred that the *g*-CNN synthesized at lower temperature can be used as a potential material for degrading methylene blue dye.

## CONFLICT OF INTEREST

The authors declare that there is no conflict of interests regarding the publication of this article.

## REFERENCES

1. B. Lellis, C.Z. Fávaro-Polonio, J.A. Pamphile and J.C. Polonio, *Biotechnol. Res. Innov.*, **3**, 275 (2019); https://doi.org/10.1016/j.biori.2019.09.001
2. M.I. Din, R. Khalid, J. Najeeb and Z. Hussain, *J. Clean. Prod.*, **298**, 126567 (2021); https://doi.org/10.1016/j.jclepro.2021.126567
3. P.O. Oladoye, T.O. Ajiboye, E.O. Omotola and O.J. Oyewola, *Results Eng.*, **16**, 100678 (2022); https://doi.org/10.1016/j.rineng.2022.100678
4. D.R. Paul and S.P. Nehra, *Environ. Sci. Pollut. Res. Int.*, **28**, 3888 (2021); https://doi.org/10.1007/s11356-020-09432-6
5. X. Luo, H. Liang, F. Qu, A. Ding, X. Cheng, C.Y. Tang and G. Li, *Chemosphere*, **200**, 237 (2018); https://doi.org/10.1016/j.chemosphere.2018.02.113
6. J. Hou, Y. Wang, J. Zhou, Y. Lu, Y. Liu and X. Lv, *Surf. Interfaces*, **22**, 100889 (2021); https://doi.org/10.1016/j.surfin.2020.100889
7. L. Suhadolnik, A. Pohar, U. Novak, B. Likozar, A. Miheliè and M. Èeh, *J. Ind. Eng. Chem.*, **72**, 178 (2019); https://doi.org/10.1016/j.jiec.2018.12.017
8. J. Huang, L. Peng, G. Zeng, X. Li, Y. Zhao, L. Liu, F. Li and Q. Chai, *Sep. Purif. Technol.*, **125**, 83 (2014); https://doi.org/10.1016/j.seppur.2014.01.020

9. O. Kazak, Y.R. Eker, I. Akin, H. Bingol and A. Tor, *J. Environ. Chem. Eng.*, **5**, 2639 (2017); https://doi.org/10.1016/j.jece.2017.05.018
10. A. Kumar and G. Pandey, *Mater. Sci. Eng. Int. J.*, **1**, 106 (2017); https://doi.org/10.15406/mseij.2017.01.00018
11. M. Rochkind, S. Pasternak and Y. Paz, *Molecules*. **20**, 88 (2015); https://doi.org/10.3390/molecules20010088
12. W. Yang, K. Ding, G. Chen, H. Wang and X. Deng, *Molecules*, **28**, 2796 (2023); https://doi.org/10.3390/molecules28062796
13. N. Gogoi, G. Borah, P.K. Gogoi and T.R. Chetia, *Chem. Phys. Lett.*, **692**, 224 (2018); https://doi.org/10.1016/j.cplett.2017.12.015
14. J.F. Cruz-Filho, T.M.S. Costa, M.S. Lima, L.J. Silva, R.S. Santos, L.S. Cavalcante, E. Longo and G.E. Luz Jr., *J. Photochem. Photobiol. A: Chem.*, **377**, 14 (2019); https://doi.org/10.1016/j.jphotochem.2019.03.031
15. M. Aggarwal, S. Basu, N.P. Shetti, M.N. Nadagouda, E.E. Kwon, Y.-K. Park and T.M. Aminabhavi, *Chem. Eng. J.*, **425**, 131402 (2021); https://doi.org/10.1016/j.cej.2021.131402
16. X. Song, M. Wang, W. Liu, X. Li, Z. Zhu, P. Huo and Y. Yan, *Appl. Surf. Sci.*, **577**, 151810 (2022); https://doi.org/10.1016/j.apsusc.2021.151810
17. Y. Qin, G. Dong, L. Zhang, G. Li and T. An, *Environ. Res.*, **195**, 110880 (2021); https://doi.org/10.1016/j.envres.2021.110880
18. M.A. Gondal, A. Lais, M.A. Dastageer, D. Yang, K. Shen and X. Chang, *Int. J. Energy Res.*, **41**, 2162 (2017); https://doi.org/10.1002/er.3777
19. L. Ma, H. Fan, M. Li, H. Tian, J. Fang and G. Dong, *J. Mater. Chem. A Mater. Energy Sustain.*, **3**, 22404 (2015); https://doi.org/10.1039/C5TA05850C
20. L. Lin, H. Ou, Y. Zhang and X. Wang, *ACS Catal.*, **6**, 3921 (2016); https://doi.org/10.1021/acscatal.6b00922
21. M. Ismael, Y. Wu, D.H. Taffa, P. Bottke and M. Wark, *New J. Chem.*, **43**, 6909 (2019); https://doi.org/10.1039/C9NJ00859D
22. Z. Zhang, Y. Zhang, L. Lu, Y. Si, S. Zhang, Y. Chen, K. Dai, P. Duan, L. Duan and J. Liu, *Appl. Surf. Sci.*, **391**, 369 (2017); https://doi.org/10.1016/j.apsusc.2016.05.174
23. H. Dou, D. Long, S. Zheng and Y. Zhang, *Catal. Sci. Technol.*, **8**, 3599 (2018); https://doi.org/10.1039/C8CY00904J
24. T.K.A. Nguyen, T.T. Pham, H. Nguyen-Phu and E.W. Shin, *Appl. Surf. Sci.*, **537**, 148027 (2021); https://doi.org/10.1016/j.apsusc.2020.148027
25. A.A. Yadav, S.W. Kang and Y.M. Hunge, *J. Mater. Sci. Mater. Electron.*, **32**, 15577 (2021); https://doi.org/10.1007/s10854-021-06106-y
26. Y. Cui, Y. Tang and X. Wang, *Mater. Lett.*, **161**, 197 (2015); https://doi.org/10.1016/j.matlet.2015.08.106
27. S.P. Pattnaik, A. Behera, R. Acharya and K. Parida, *J. Environ. Chem. Eng.*, **7**, 103456 (2019); https://doi.org/10.1016/j.jece.2019.103456
28. H. Jigyasa, H. Singh and J.K. Rajput, *Food Chem.*, **343**, 128451 (2021); https://doi.org/10.1016/j.foodchem.2020.128451
29. Q. Zhao, W. Wu, X. Wei, S. Jiang, T. Zhou, Q. Li and Q. Lu, *Sens. Actuators B Chem.*, **248**, 673 (2017); https://doi.org/10.1016/j.snb.2017.04.002
30. G. Kesavan and S.M. Chen, *Diamond Rel. Mater.*, **108**, 107975 (2020); https://doi.org/10.1016/j.diamond.2020.107975
31. A.O. Idris, E.O. Oseghe, T.A.M. Msagati, A.T. Kuvarega, U. Feleni and B. Mamba, *Sensors*, **20**, 5743 (2020); https://doi.org/10.3390/s20205743
32. Y. Gong, M. Li, H. Li and Y. Wang, *Green Chem.*, **17**, 715 (2015); https://doi.org/10.1039/C4GC01847H
33. M. Baar and S. Blechert, *Chem. Eur. J.*, **21**, 526 (2015); https://doi.org/10.1002/chem.201405505
34. N.D. Shcherban, P. Mäki-Arvela, A. Aho, S.A. Sergiienko, P.S. Yaremov, K. Eränen and D.Y. Murzin, *Catal. Sci. Technol.*, **8**, 2928 (2018); https://doi.org/10.1039/C8CY00253C
35. B. Kurpil, B. Kumru, T. Heil, M. Antonietti and A. Savateev, *Green Chem.*, **20**, 838 (2018); https://doi.org/10.1039/C7GC03734A
36. D.R. Paul, R. Sharma, S.P. Nehra and A. Sharma, *RSC Adv.*, **9**, 15381 (2019); https://doi.org/10.1039/C9RA02201E
37. H. Montigaud, B. Tanguy, G. Demazeau, I. Alves and S. Courjault, *J. Mater. Sci.*, **35**, 2547 (2000); https://doi.org/10.1023/A:1004798509417
38. Q. Guo, Y. Xie, X. Wang, S. Lv, T. Hou and X. Liu, *Chem. Phys. Lett.*, **380**, 84 (2003); https://doi.org/10.1016/j.cplett.2003.09.009
39. Y.J. Bai, B. Lü, Z.-G. Liu, L. Li, D.-L. Cui, X.-G. Xu and Q.-L. Wang, *J. Cryst. Growth*, **247**, 505 (2003); https://doi.org/10.1016/S0022-0248(02)01981-4
40. P. Praus, A. Smýkalová, K. Foniok, V. Matijka, M. Kormunda, B. Smetana and D. Cvejn, *Appl. Surf. Sci.*, **529**, 147086 (2020); https://doi.org/10.1016/j.apsusc.2020.147086
41. B.K. Choudhury and S.K. Gogoi, *Nano-Structures and Nano-Objects*, **26**, 100704 (2021); https://doi.org/10.1016/j.nanoso.2021.100704
42. X. Cai, J. He, L. Chen, K. Chen, Y. Li, K. Zhang, Z. Jin, J. Liu, C. Wang, X. Wang, L. Kong and J. Liu, *Chemosphere*, **171**, 192 (2017); https://doi.org/10.1016/j.chemosphere.2016.12.073
43. P. Choudhary, A. Bahuguna, A. Kumar, S.S. Dhankhar, C.M. Nagaraja and V. Krishnan, *Green Chem.*, **22**, 5084 (2020); https://doi.org/10.1039/D0GC01123A
44. Q. Gu, Z. Gao and C. Xue, *Small*, **12**, 3543 (2016); https://doi.org/10.1002/smll.201600181
45. Y. Wang, H. Wang, F. Chen, F. Cao, X. Zhao, S. Meng and Y. Cui, *Appl. Catal. B*, **206**, 417 (2017); https://doi.org/10.1016/j.apcatb.2017.01.041
46. S. Liu, D. Li, H. Sun, H.M. Ang, M.O. Tadé and S. Wang, *J. Colloid Interface Sci.*, **468**, 176 (2016); https://doi.org/10.1016/j.jcis.2016.01.051
47. D. Fu, G. Han, F. Liu, Y. Xiao, H. Wang, R. Liu and C. Liu, *Mater. Sci. Semicond. Process.*, **27**, 966 (2014); https://doi.org/10.1016/j.mssp.2014.08.004